

## Effect of metal impurities concentration on electrical properties in N-type Recharged-Czochralski silicon

Zhiqiang Hu <sup>a,b</sup>, Mu Cong <sup>a,b</sup>, Xinyu Zhang <sup>c</sup>, Jiayan Li <sup>a,b</sup>, Jiangang Zhang <sup>a,b</sup>, Yi Tan <sup>a,b</sup>, Ziyang Ou <sup>c</sup>, Yangjun Chen <sup>c</sup>, Changming Liu <sup>c</sup>, Dachuan Jiang <sup>a,b</sup>, Pengting Li <sup>a,b,\*</sup>

<sup>a</sup> Key Laboratory of Materials Modification by Laser, Ion and Electron Beams (Dalian University of Technology), Ministry of Education, School of Materials Science and Engineering, Dalian, 116024, China

<sup>b</sup> Key Laboratory for Energy Beam Metallurgy and Advanced Materials Preparation of Liaoning Province, Dalian, 116024, China

<sup>c</sup> Jinko Solar Co., Ltd, Jiangxi, Shangrao, 334100, China



### ARTICLE INFO

**Keywords:**  
Czochralski silicon  
Solar cells  
Metal impurity  
Minority carrier lifetime

### ABSTRACT

The electrical properties of N-type Recharged-Czochralski (RCz) silicon solar cells are significantly affected by the concentration of metal impurities in the silicon materials. In this work, several N-type RCz silicon ingots were grown using feedstock with different impurities concentration, and the distribution of minority carrier lifetime was tested. It was discovered that a broader range of feedstock impurity concentrations resulted in high and stable minority carrier lifetime of the ingots. Solar cells made from these ingots had an average efficiency of over 24.57%. Meanwhile, the results of impurities segregation calculation and solar cells electroluminescence(EL) test were given. The results indicated that ring defects were the primary cause of differences in electrical properties among silicon ingots produced from feedstock with varying impurity concentrations. Further, the process window to produce high efficiency N-type Czochralski(Cz) silicon solar cells was broadened, and the production cost could be reduced.

### 1. Introduction

The global population's expansion is leading to a higher demand for affordable energy, but unfortunately, this demand relies heavily on fossil fuels [1], exacerbating greenhouse gas emissions and the ongoing climate crisis. To address these challenges, solar energy has emerged as a crucial solution, offering clean and renewable advantages [2,3]. Currently, crystalline silicon solar energy dominates the market, capturing over 90% of the mainstream market share [4]. Within this sector, monocrystalline silicon batteries have experienced rapid development in recent years thanks to advancements in battery structure and slicing technology, gradually occupying the main market share [5,6]. However, facing the rapid development of monocrystalline silicon solar cells, how to reduce production costs in the industrialization process and produce high-performance monocrystalline silicon batteries at low cost has become a current industry concern.

However, in industrial production, cost reduction often involves utilizing relatively low-purity silicon materials, which consequentially introduces numerous metal impurities to the ingot. Although, Bandana

Singha et al.'s research shows that n-type solar cells have a certain tolerance to some metal impurities (such as Fe, Ti et al.) [7], it is important to note that certain metal impurities including Co, Cr, and Ti still exhibit strong recombination activity in n-type silicon [8]. To address this issue, it has been suggested that methods such as Phosphorus diffusion gettering be employed to minimize metal impurity losses and improve the electrical properties of solar cells [9]. However, the gettering process involves the diffusion of impurities, so for certain metal impurities with slow diffusion coefficients, it may not produce satisfactory results [10]. Meanwhile, in the process of industrial production, the prolonged gettering not only leads to increased production costs but also hampers production capacity. By reducing the time taken for gettering, substantial improvements can be made to production efficiency. Therefore, currently controlling the impurity content in raw materials and optimizing the selection window have become the main ways for the industry to reduce production costs.

Similarly, oxygen in Czochralski silicon can also negatively impact its electrical properties under certain conditions. The increase of oxygen content in Cz silicon may lead to the thermal donor effect of oxygen and

\* Corresponding author. School of Materials Science and Engineering, Dalian University of Technology, No. 2 Linggong Road, Ganjingzi District, Dalian, 116024, China.

E-mail address: [ptli@dlut.edu.cn](mailto:ptli@dlut.edu.cn) (P. Li).

the increase of oxygen precipitation content [11,12]. Meanwhile, numerous research results have shown that oxygen precipitation can lead to resistivity distortion of silicon wafers and affect the conversion efficiency of solar cells [13,14]. Besides, recent studies showed that the ring defects which have a significant effect on the electrical properties of Cz silicon were also likely to be related to oxygen content [15,16]. Some studies believed that ring defect in Cz silicon was caused by oxygen precipitation [17]. Thus, the primary approach for managing oxygen levels in high-performance Cz silicon involves utilizing a combination of thermal field optimization and high-purity auxiliary materials, which will undoubtedly raise the production costs. In brief, enhancing the purity of feedstocks appears to be the most straightforward and efficient method for mitigating the negative influence of metal and oxygen impurities on solar cell performance. However, due to inadequate exploration on the impacts of these impurities on CZ silicon's electrical properties, there is no definitive criteria for choosing feedstocks. Consequently, the industry relies on high-purity feedstocks, making cost reduction challenging.

In this work, based on the production data from 2021, the relationship between metal impurities concentration, oxygen content and electrical properties in high performance Cz silicon was studied. Through the impurities concentration calculation and the characterization of the minority carrier lifetime of the silicon ingots, combined with the EL test of solar cells, the reasons for the differences in electrical properties were revealed. Based on the test result of minority carrier lifetime of the ingots and the statistical efficiency of solar cells produced by RCz, a broader feedstock window to produce high efficiency N-type Cz silicon was proposed, which will provide guidance and reference for reducing high efficiency N-type solar cells production costs.

## 2. Materials and experiment

### 2.1. Feedstocks

The purpose of this work is to investigate the impact of metal impurities on the conversion efficiency of solar cells produced, thereby expanding the process window for feedstock selection. To achieve this goal, high-purity silicon materials named A, B, and C were used as feedstocks, as well as mixtures of these materials with impurities containing silicon materials at varying ratios. The total concentration of hazardous impurity elements - Al, V, Cr, Mn, Fe, Ni, Cu - in the feedstocks was characterized [18–20]. Detection of metal impurities was performed through the use of an inductively coupled plasma mass

spectrometer (ICP-MS), and the resulting data were presented in Fig. 1.

In addition, testing was performed on the content of different impurities in the feedstocks, and the resulting data were presented in Table 1.

### 2.2. Ingot production process

For this work, the ingots were mainly produced using industrial RCz ingot furnaces shown in Fig. 2 (a). The equipment included the main furnace chamber, auxiliary furnace chamber, seed crystal lifting and rotating mechanism, and equipment base frame. The outermost layer of the Cz furnace had multiple layers of carbon felt to maintain the internal thermal field, while the inner layer consisted of a graphite heater that provided the high temperature needed for melting. During production process, the mixed silicon material is placed inside the crucible and heated by a graphite heater until it melts. Then, slowly contact the seed crystal with a fixed crystal phase with the surface of the melt, promoting the epitaxial growth of the melt on the surface of the seed crystal. During the process, the seed crystal axis and the melt crucible rotate simultaneously to maintain a stable contact interface.

As shown in Fig. 2 (b), during production process, the mixed silicon material is placed inside the crucible and heated by the graphite heater until it melts. Then, slowly contact the seed crystal with a fixed crystal phase with the surface of the melt, promoting the epitaxial growth of the melt on the surface of the seed crystal. During the process, the seed crystal axis and the melt crucible rotate simultaneously to maintain a stable contact interface. After successfully completing the crystallization process, dislocations are first removed from the monocrystalline silicon through the necking process, and then gradually coarsened to the preset diameter, and maintained until the silicon ingot is lifted. Lift the silicon ingot that has already solidified out of the main furnace chamber. Repeat the above process to complete the multi ingots lifting. According to the production sequence of monocrystalline silicon rods, ingot 1, ingot 2, ingot 3 and so on are named respectively. The relevant production parameters are shown in Table 2.

To investigate the effect of oxygen content on minority carrier lifetime in n-type Cz monocrystalline silicon produced by RCz method, the detailed distribution of oxygen content in silicon ingots was first characterized. Take samples every 25% of the axial solidification length ratio of the crystal ingot after cutting and processing, and take samples every 10% of the radial length ratio for point detection. Similarly, for the minority carrier lifetime, take samples every 25% of the axial solidification length ratio of the silicon ingot after cutting and processing, and take samples every 20% of the radial length ratio for point detection, as shown in Fig. 2 (c).

### 2.3. Analysis methods

The interstitial oxygen concentration([O<sub>i</sub>]) of the ingots was characterized by Fourier transform infrared spectroscopy (FTIR). The Bulk minority carrier lifetime of the ingots was characterized by BCT-400 using the quasi-steady-state photoconductivity (QSSPC) method. The resistivity of the samples was tested by four-probe resistivity tester in the experiment. To reflect the impact of impurities concentration on the conversion efficiency of the solar cells, the average efficiency of solar cells made from each group was counted. In addition, to study the differences in electrical properties of different groups, the proportional statistics of ring defects were counted through EL test (By observing the number of silicon wafers with ring defects and dividing it by the total production amount). For the specific details of the above detection methods, please refer to the supplementary data I. The workflow of this work can be summarized as shown in Fig. 3.

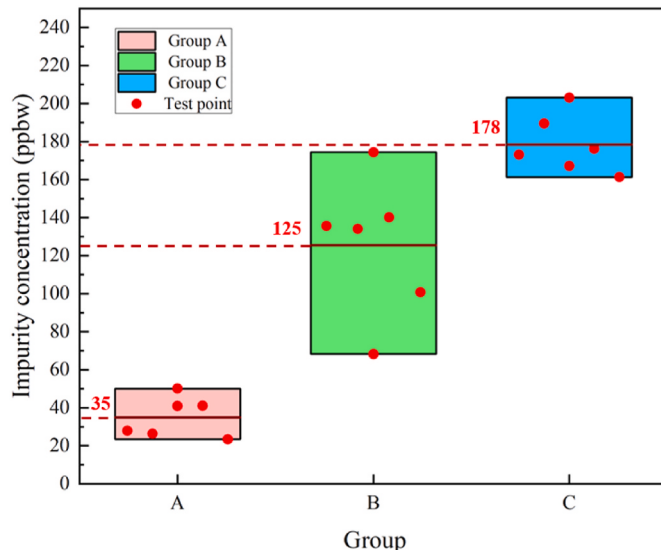


**Fig. 1.** Distribution of impurities in each group of feedstocks.

**Table 1**

Content of metal impurities in different group of feedstocks.

Element	Al	V	Cr	Mn	Fe	Ni	Cu	Total(ppbw)
Group A	6.75	0.11	4.61	3.11	17.46	2.51	0.42	34.98
Group B	37.73	0.21	8.78	3.68	67.68	4.37	3.05	125.74
Group C	46.28	0.30	6.69	3.90	112.33	4.23	4.33	178.36

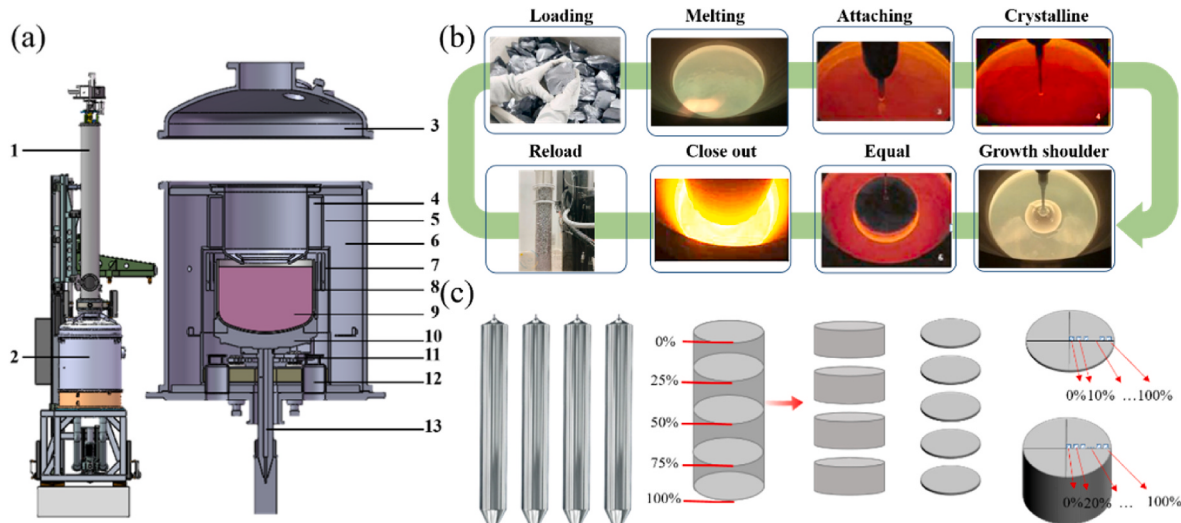


**Fig. 2.** Schematic diagram of ingot production process and sampling analysis location: (a): Schematic diagram of Cz crystal silicon furnace; (1: Auxiliary furnace chamber; 2: Main furnace Chamber; 3: Upper insulation cover; 4: Flow guide cylinder; 5: Insulated cylinder; 6: Insulation felt; 7: Main heater; 8: Quartz crucible; 9: Silicon melt; 10: Crucible holder; 11: Bottom heater; 12: Vent-hole; 13: Crucible support shaft) (b): Process production process; (c): Schematic diagram of sampling location.

**Table 2**

Growth parameters of Cz silicon.

Doped element	Head resistivity ( $\Omega\text{-cm}$ )	diameter (mm)	smelting time (h)	Lifting rate (mm/h)	Seed rotation (r/min)	Crucible rotation (r/min)
P	1.2–1.4	230	8–12	100~120	7~8	8

### 3. Results & discussion

#### 3.1. Minority carrier lifetime and [Oi] distribution of 4 ingots continuous growth by RCz

In the production of Cz silicon, the presence of oxygen from the quartz crucible is inevitable, and this may have an effect on the minority carrier lifetime. Therefore, in this part, selecting Group B as the raw material and continuously producing four crystal silicon rods through the RCz technology. The characterization of four continuously grown RCz ingots included the analysis of the minority carrier lifetime, resistivity, [Cs], and [Oi] distributions, as illustrated in Figs. 4 and 5. In Fig. 4, it can be observed that for each ingot, as the solidification fraction increases, both the minority carrier lifetime and resistivity decrease along the growth direction. Furthermore, as the number of ingots increases, the minority carrier lifetime decreases for each subsequent ingot, while the resistivity of the ingot head remains relatively stable. Specifically, the minority carrier lifetime of the ingot head decreased from 6900  $\mu\text{s}$  in the first ingot to 4300  $\mu\text{s}$  in the fourth ingot, whereas the resistivity remained consistently around 1.1–1.3  $\Omega\text{ cm}$  (with the resistivity of the first three rods remaining stable around 1.3  $\Omega\text{ cm}$ ).

Because of its high effective segregation coefficient, [Oi] has a tendency to accumulate in the ingot during solidification, which leads to a gradual decrease in oxygen content in the single crystal silicon rod. The primary source of oxygen impurities during production usually comes from quartz crucibles. To reduce their infiltration into the silicon rod,

techniques such as crucible and crystal rotation are used. However, it is essential to reduce both crystal and crucible rotation speeds after the single crystal rod pulling stage to ensure the inhibiting effect on oxygen impurity infiltration is not undermined, thus leading to an abnormal increase in oxygen impurity content at the tail end. As indicated in Fig. 5, [Oi] decreases gradually with increasing solidification ratio in the growth direction, but some crystal ingots show an opposite trend with a rise in [Oi] at the tail, and the distribution of [Oi] increases with higher numbers of ingots. While [Oi] is typically thought to negatively affect minority carrier lifetime, this study's results indicate that continuous crystal growth's changes in [Oi] do not significantly impact it. Further characterization is necessary to verify this finding, as detailed in Supplemental Material II.

Furthermore, minority carrier lifetime and [Oi] distributions of one of the RCz crystals was characterized in detail. Group B raw materials were selected for production in this experiment, due to the loss of samples during the testing process. Ingot 3 in the later stage of solidification was selected for detection and analysis, to better understand the influence of oxygen, since oxygen mainly comes from quartz crucibles. As shown in Fig. 6(a), the axial and radial minority carrier lifetime of the ingot is characterized, respectively. The X and Y axes represent the axial and radial directions in the ingot and represent the minority carrier lifetime corresponding to that position. The minority carrier lifetime of the entire ingot ranged from the highest value of 6300  $\mu\text{s}$  to the lowest value of 3800  $\mu\text{s}$ . In the axial direction of ingot, from center to edge, minority carrier lifetime decreased with the increase of the solidification

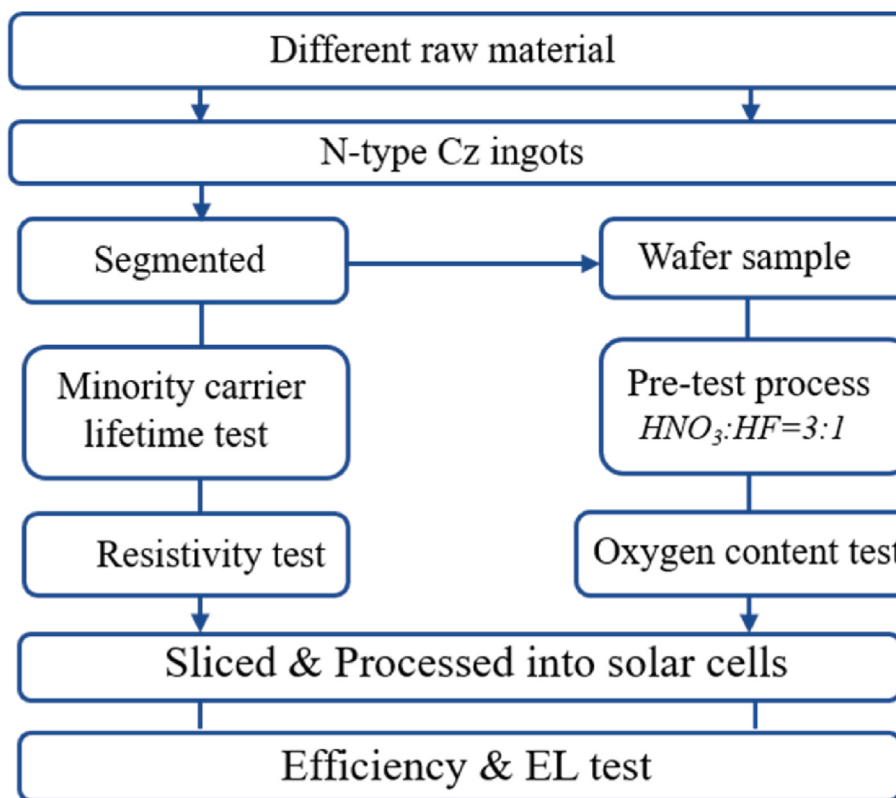


**Fig. 3.** Processing and testing flow chart.

ratio, and the difference between the head and tail was greater than 2500  $\mu\text{s}$ . In the radial direction, the minority carrier lifetime changed gently, less than 600  $\mu\text{s}$ . The distribution of minority carrier lifetime in the crystal ingot was lower at the center and higher at the edge. For a crystal ingot, the change in the solidification direction of minority carrier lifetime is significantly higher than that of the radial direction. Minority carrier lifetime mainly varies in the axial direction. (Please refer to Supplement Material II for detailed testing data).

As for [O<sub>i</sub>], as shown in Fig. 6 (b), the axial and radial [O<sub>i</sub>] of the ingot was characterized respectively. The [O<sub>i</sub>] of the whole ingot was approximately from the highest 10.43 ppma to the lowest 2.60 ppma. In the axial direction of ingot, [O<sub>i</sub>] decreased with the increase of the solidification ratio, and the difference between the head and tail was greater than 7ppma. In the radial direction, [O<sub>i</sub>] changed gently, less than 2 ppma. The distribution of [O<sub>i</sub>] in the crystal ingot was lower at the center and higher at the edge. For a crystal ingot, the change in the solidification direction of [O<sub>i</sub>] was significantly higher than that of the radial direction. (Please refer to Supplement Material II for detailed testing data).

In summary, in a silicon ingot, the change in minority carrier lifetime and [O<sub>i</sub>] is mainly in the direction of the solidification ratio, and the change in the radial direction is small. There is no significant correlation between the distribution of [O<sub>i</sub>] and the distribution of minority carrier lifetime. The distribution of minority carrier lifetime seems to be more affected by other factors.

### 3.2. Minority carrier lifetime distribution of RCz ingots with different metal impurities concentration

Another factor that may have a significant effect on the minority carrier lifetime of silicon ingots is the content of metal impurities [21, 22]. To further explore the effect of impurities concentration on minority carrier lifetime of RCz crystal ingots, the minority carrier lifetime distribution of three groups of feedstock with different impurities

concentration was analyzed. Groups A, B, and C, which represented 4 ingots continuously grew from feedstock with low impurities concentration, medium impurities concentration and high impurities concentration.

As shown in Fig. 7, it reflects the minority carrier lifetime distribution of ingots grown with different feedstock. The distribution of the minority carrier lifetime of each ingot continues the trend of change of the minority carrier lifetime in an individual ingot, where the minority carrier lifetime decreased with the increase of solidification ratio in the axial direction. And in the RCz ingots continuously grown from the same feedstock, the trend of change of 4 ingots was also the same as described above. As the number of growth ingots increased, the distribution of minority carrier lifetime decreased.

The use of feedstock with different impurity concentrations had varying effects on the distribution of minority carrier lifetime in RCz continuously grown ingots. There was an overall gap in the distribution of the minority carrier lifetime between RCz ingots grown from different groups. The higher the impurities concentration of the feedstock, the lower the overall minority carrier lifetime distribution of the grown ingots. In group A, the maximum head minority carrier lifetime was about 9000  $\mu\text{s}$ , while in group B, the maximum head minority carrier lifetime was about 7000  $\mu\text{s}$ , and in group C, the head minority carrier lifetime was only about 5300  $\mu\text{s}$ . In order to accurately assess the influence of impurity content on changes in minority carrier lifetime during the solidification process, this study conducted a comparative analysis. Specifically, the minority carrier lifetime of the first rod, which was produced using raw materials with varying impurity contents, was examined at different solidification heights, and the trend of minority carrier lifetime changes was determined through fitting analysis. The fitting results were shown in Fig. 7 (d), indicating significant differences in minority carrier lifetime changes between different groups. In Group A, characterized by the highest minority carrier lifetime, a rapid decline was observed with increasing solidification height, at a rate of  $-3.31 \mu\text{s}/\text{mm}$ . In Group B, despite having a relatively lower minority carrier

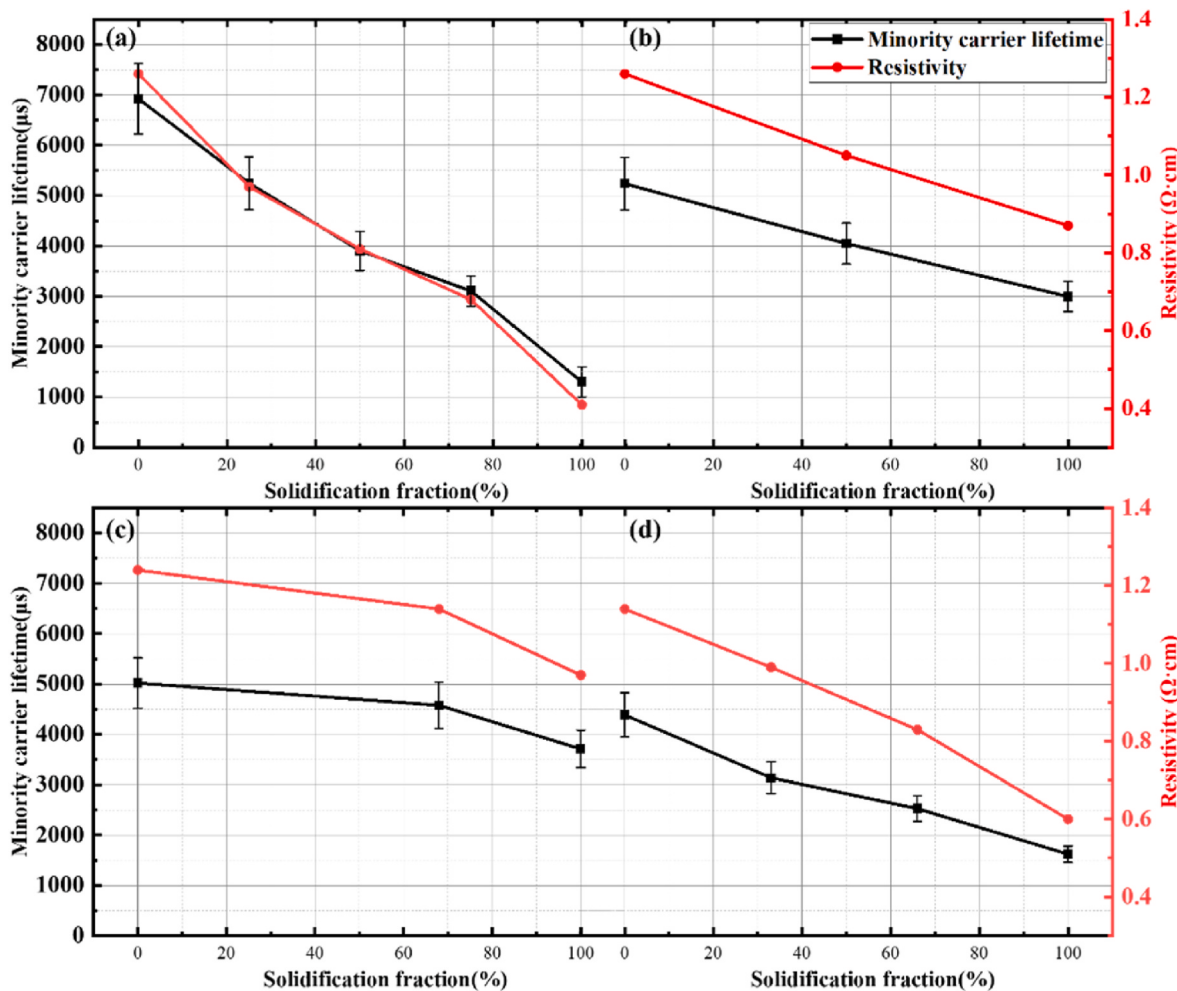


**Fig. 4.** Distribution of minority carrier lifetime and resistivity in RCz continuous growth crystal ingots: (a) Ingot 1; (b) Ingot 2; (c) Ingot 3; (d) Ingot 4.

lifetime, the rate of change was somewhat attenuated, at  $-2.16 \mu\text{s/mm}$ . Within Group C, the minority carrier lifetime started at a comparably lower value but exhibited a less pronounced change rate within the crystal rod as solidification height increased, recording only  $-0.91 \mu\text{s/mm}$ . The phenomenon is believed to occur because, with low levels of metal impurities, their deep-level effect is more pronounced, leading to a rapid decline in minority carrier lifetime as metal impurity content increases. However, when the metal impurity content surpasses a certain threshold, the deep-level effect becomes saturated, thus reducing the semiconductor's sensitivity to changes in metal impurity content and having a minimal impact on minority carrier lifetime. Therefore, to some extent, this has also led to one of the research topics in this article, which is to broaden the selection of raw materials while maintaining stable performance.

In summary, the distribution of minority carrier lifetime is related to the content of metal impurities. The minority carrier lifetime distribution of RCz ingots grown by feedstock with different metal impurity content was different. Group B, compared to other groups, maintained a high and relatively stable minority carrier lifetime distribution while appropriately widening the range of metal impurities concentration in the feedstock."

### 3.3. Electrical properties of RCz silicon with different metal impurities concentration

The impact of metal impurity content on the electrical properties of RCz silicon was investigated by processing different sets of ingots from

section 3.2 into TOPcon structured solar cells and conducting tests to determine their average photoelectric conversion efficiency.

As shown in Fig. 8, the efficiency of solar cell production using different groups of feedstock was measured. With the change in impurity concentration in the feedstock, the average efficiency of solar cells varies in different degrees. Compared with group A, the efficiency of group B was only 0.03% lower. For group C, although the difference of the impurity content was relatively small compared with group B, its efficiency decreased about 0.20%. Under the premise of properly broadening the concentration of metal impurities, group B achieved a high and relatively stable minority carrier lifetime, and its efficiency was high, reaching 24.57%. Additionally, a certain proportion of solar cells with ring defects were detected through the EL test in group C.

As shown in Table 3, the proportion of ring defects in different groups and solar cells efficiency was counted. Compared with other groups, there was a higher proportion of ring defects in group C. It is worth noting that there exists a standard for the proportion of environmental defects in the production process, which is set at a maximum of 0.15%. If the proportion shown in the table falls below 0.15%, the batch is considered qualified, and the specific proportion is not recorded. This had a good fitting with the change of efficiency. It will be discussed later.

In summary, RCz silicon ingots containing various metal impurities exhibited significant differences electrical properties and minority carrier lifetime. These differences could be attributed to the distribution of metal impurities in the ingot and melt during crystal growth. In addition, the proportion of solar cells with ring defects was different in

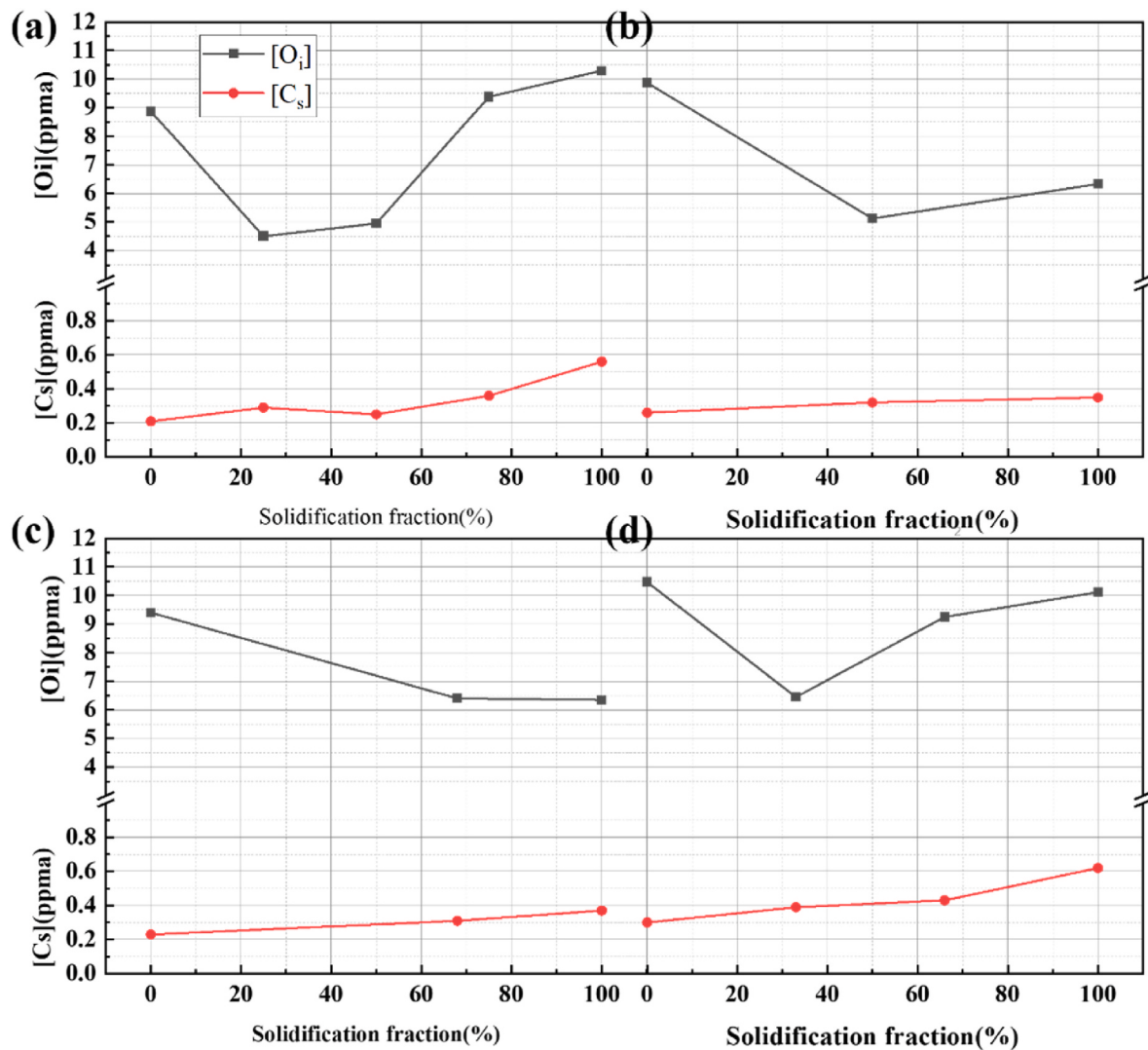


Fig. 5. Distribution of [O<sub>i</sub>] & [Cs] in RCz continuous growth crystal ingots: (a) Ingot 1 (b) Ingot 2 (c) Ingot 3 (d) Ingot 4.

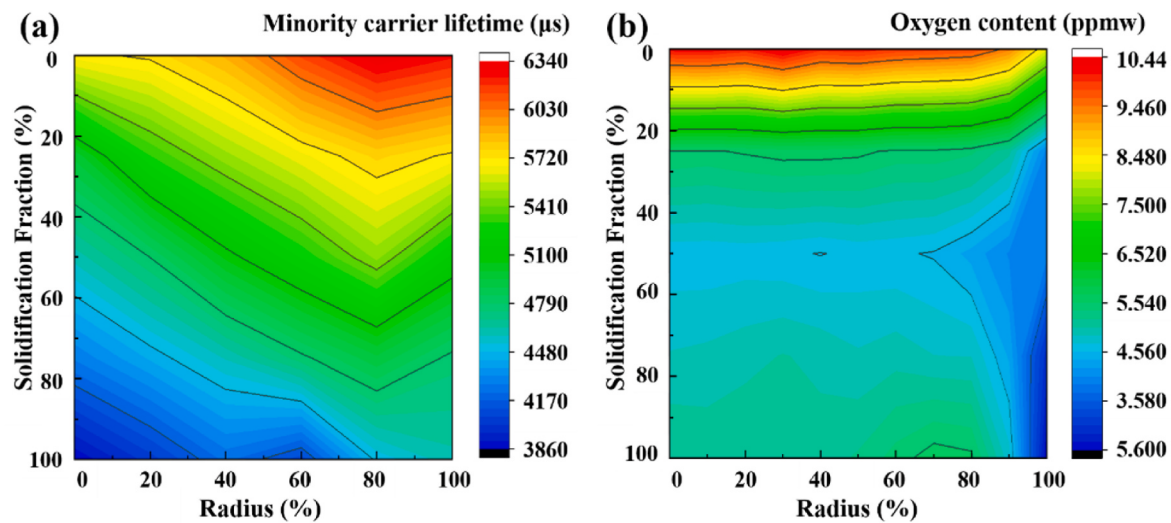
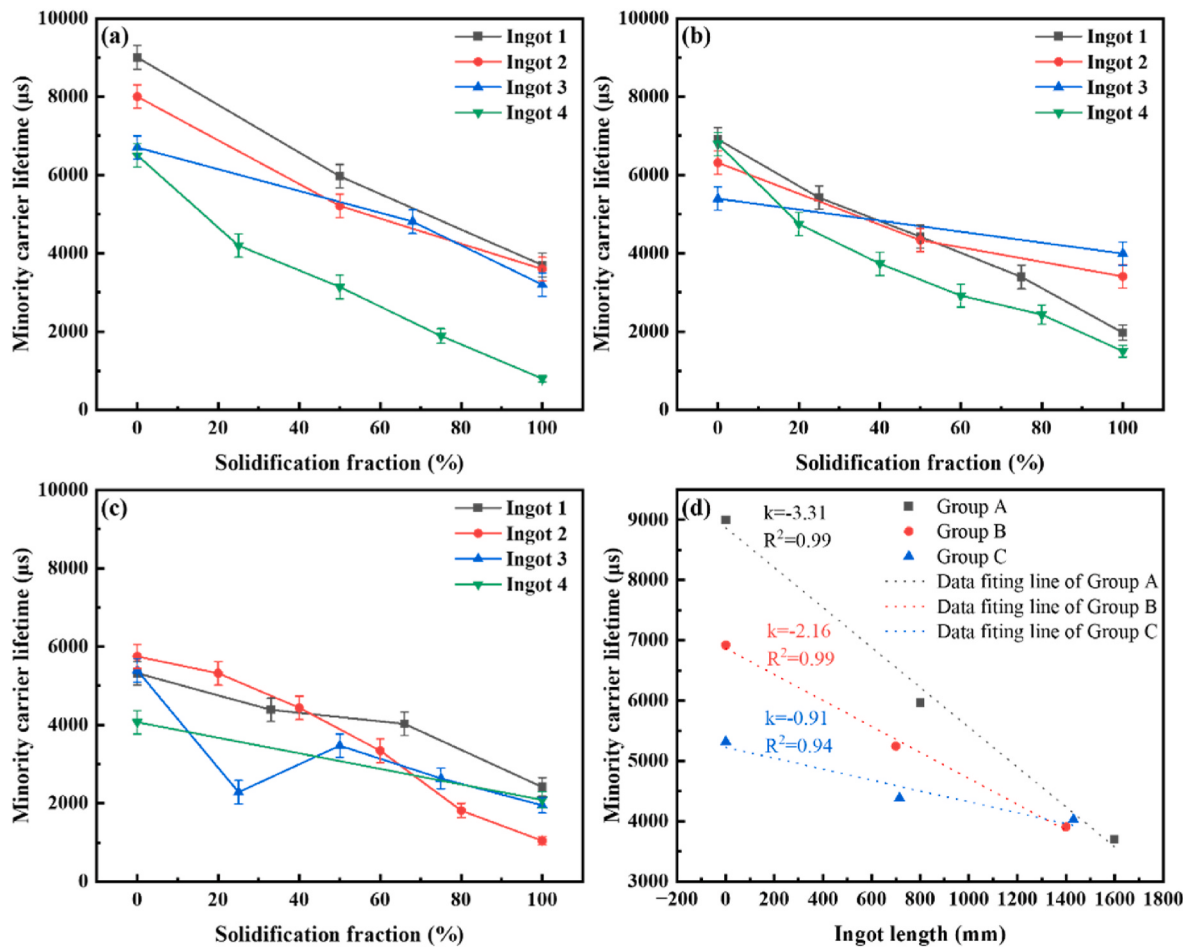
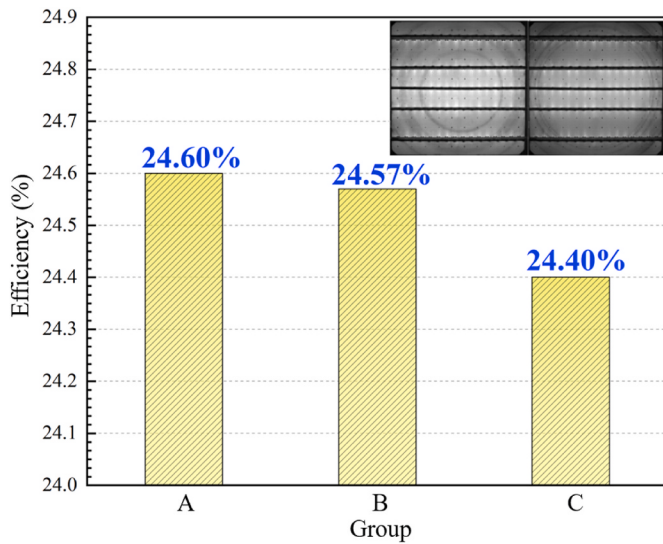


Fig. 6. Analysis results of ingot 3 produced through Group B (a) Distribution of minority carrier lifetime; (b) Distribution of [O<sub>i</sub>].



**Fig. 7.** Minority carrier lifetime distribution of ingots grown with different feedstock (a) group A; (b) group B; (c) group C; (d) Change ratio of minority carrier lifetime in the head.



**Fig. 8.** Efficiency of solar cells made from feedstock with different impurities concentration.

**Table 3**  
Solar cells efficiency & ring defect.

Group	A	B	C
Eff (%)	24.60	24.57	24.40
Uoc (V)	0.71	0.71	0.71
Isc (A)	11.0	11.0	11.0
FF(%)	84.0	83.8	82.9
Wafer count	30,456	28,549	30,051
Ring defect proportion (%)	<0.15	<0.15	3.86

different groups, which may be intrinsically related to the concentration of metal impurities.

#### 3.4. Effect of impurities segregation

During the growing process of monocrystalline silicon ingots, feedstock is transformed from silicon melt to silicon crystal ingot. The segregation effect of impurities occurs at the solid-liquid interface, which is the key part of this transformation. Due to the segregation coefficient, the concentration of impurities entering the silicon ingot may be higher or lower than that in molten silicon. In general, the segregation coefficient  $k$  is defined as the ratio of the impurity concentration  $C_s$  in the solid phase to the impurity concentration  $C_l$  in the liquid phase, that is [23]:

$$k = \frac{C_s}{C_l} \quad (2)$$

in equilibrium conditions, for all kinds of elements with segregation coefficient less than 1 in silicon, some impurities are excluded from the solid phase according to the segregation principle in the process of crystal growing for Cz silicon. Therefore, the concentration of impurities in the solid phase is obviously much lower than that in the liquid phase.

In this work, the segregation coefficient of all kinds of metal elements which have great influence on electrical properties are far less than 1, and only a small part of them will enter the solid phase. However, with the progress of crystal growing, the enrichment of impurity elements in molten silicon leads to the continuous increase of  $C_l$  and the corresponding increase of the number of impurity atoms entering the crystal ingot, which leads to the corresponding increase of  $C_s$ . Fig. 9 shows that impurities segregation and solid-liquid interface both affect the distribution of minority carrier lifetime in RCz-grown ingots. In the solidification direction, metal impurities concentrate much more at the tail than the head due to the segregation of impurities. In the radial direction, the convex solid-liquid interface and impurities segregation cause the lifetime distribution to be low at the center and high at the edge. Hence, the minority carrier lifetime decreases continuously from the head to the tail in the axial direction and is lower in the center and higher at the edge in the radial direction.

As shown in Fig. 10, for RCz continuous crystal growing, and the feedstock are refeeded after growing an ingot. The impurities concentration of the newly added feedstock is much lower than that of the molten silicon after crystallization, which dilutes the metal impurities concentration in the molten silicon. Therefore, at the beginning of ingot growing, the impurities concentration in head of this ingot is higher than that in head of the previous ingot. But it is much lower than impurities concentration in the tail of the previous ingot. Therefore, in the continuous growing process, the minority carrier lifetime at the head of ingot decreases slightly with the number of growing ingots.

To explore the direct relationship between the metal impurities in the crystal ingot and the minority carrier lifetime, the impurity content distribution in the crystal ingots is theoretically calculated by Scheil equation and the effective segregation coefficient. The effective segregation coefficient used in impurities segregation calculation is shown in

**Table 4** [24].

To intuitively show the change of impurities concentration in the crystal ingot and silicon melt, the modified Scheil equation is as follows [25]:

$$C_s^* = C_0 \times k_0 \times (1 - f_s)^{k_0 - 1} \quad (3)$$

$$f_s = \frac{M_c}{M_r} \quad (4)$$

$C_s^*$  represents the impurity concentration of the solid phase;  $C_0$  represents the initial concentration of liquid impurities;  $k_0$  represents the segregation coefficient;  $f_s$  represents the solidification length;  $M_c$  represents the mass of crystal ingot;  $M_r$  represents the total mass of feedstock.

The theoretical calculations mentioned earlier provide the impurity content at different pulling stages, making it possible to compare the enrichment behavior of various raw materials during solidification. However, to get a clearer understanding of the relationship between minority carrier lifetime and raw material purity, the resistivity of silicon wafers cannot be overlooked. To reduce any errors introduced in the production process, this study records the minority carrier lifetime and resistivity of silicon wafers produced using different raw material purities simultaneously. By doing so, the Contour line diagram of resistivity, minority carrier lifetime, and melt impurity content can be generated through the origin, as depicted in Fig. 11 (a). Different regions in the picture represent the distribution range of ingots produced by different impurity groups. The minority carrier lifetime distributions of the three groups of feedstock with different impurities concentration were different. At the same resistivity, the minority carrier lifetime decreased with the increase of metal impurities. Selection of different impurities concentration feedstock for continuous crystal growing changes the impurities concentration in silicon melt during crystal growing. Although group A had a higher minority carrier lifetime, the utilization of regions with high minority carrier lifetime in the 300–1100 ppb range was lower (Shown in Fig. 11 (b)). On the other hand, group C exceeded the threshold of high minority carrier lifetime,

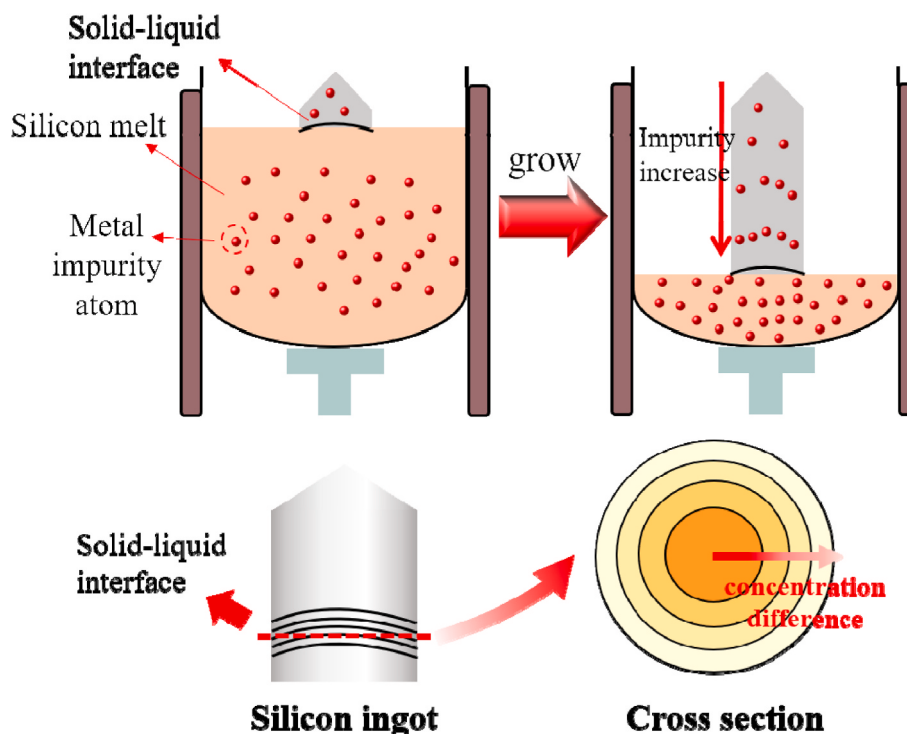


**Fig. 9.** Effect of impurity segregation and solid-liquid interface in an ingot.

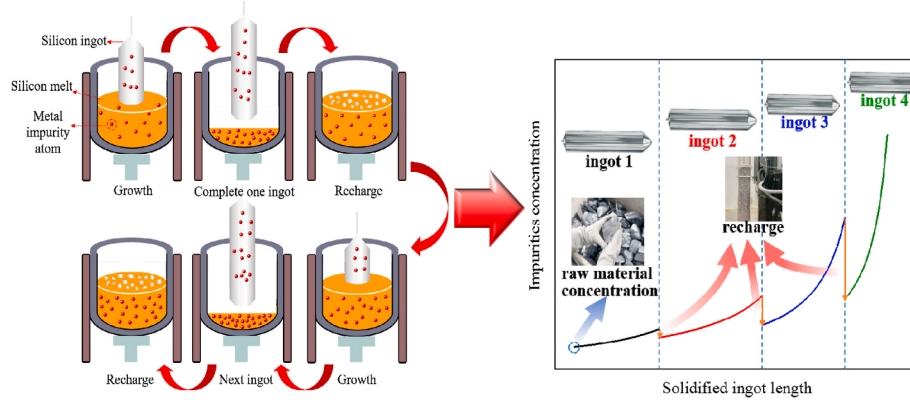


**Fig. 10.** Distribution change of metal impurities in RCz production.

**Table 4**  
Segregation coefficient of impurities in silicon.

Element	Al	V	Cr	Mn	Fe	Ni	Cu	Mo
$k_0$	$4 \times 10^{-3}$	$4 \times 10^{-6}$	1.1	1.3	6.4	3.2	$8 \times 10^{-4}$	4.5
			$\times$	$\times$	$\times$	$\times$		$\times$
				$10^{-5}$	$10^{-5}$	$10^{-6}$	$10^{-5}$	$10^{-8}$

and many regions were in the distribution area of low minority carrier lifetime, resulting in a lower overall distribution of minority carrier lifetime (Shown in Fig. 11 (d)). Group B, however, achieved a stable and relatively high minority carrier lifetime by broadening the impurity content of feedstock (Shown in Fig. 11 (c)). Group B is the superior option because it allows for better control of impurity concentration in

the molten pool during crystal growth by utilizing a range of feedstocks with varying properties, ensuring that it is situated in an area of high minority carrier lifetime. This relaxed approach to feedstock selection allows for a broader process window, which in turn creates opportunities for cost savings while maintaining an ideal balance between efficiency and cost. For further supporting data, please refer to Supplemental Material II.

### 3.5. Effect of ring defects

To explore the reasons for the significant differences in electrical properties in different groups, we further discussed the detection statistics of ring defects. According to related research, ring defects will greatly affect the electrical properties of monocrystalline silicon [16,

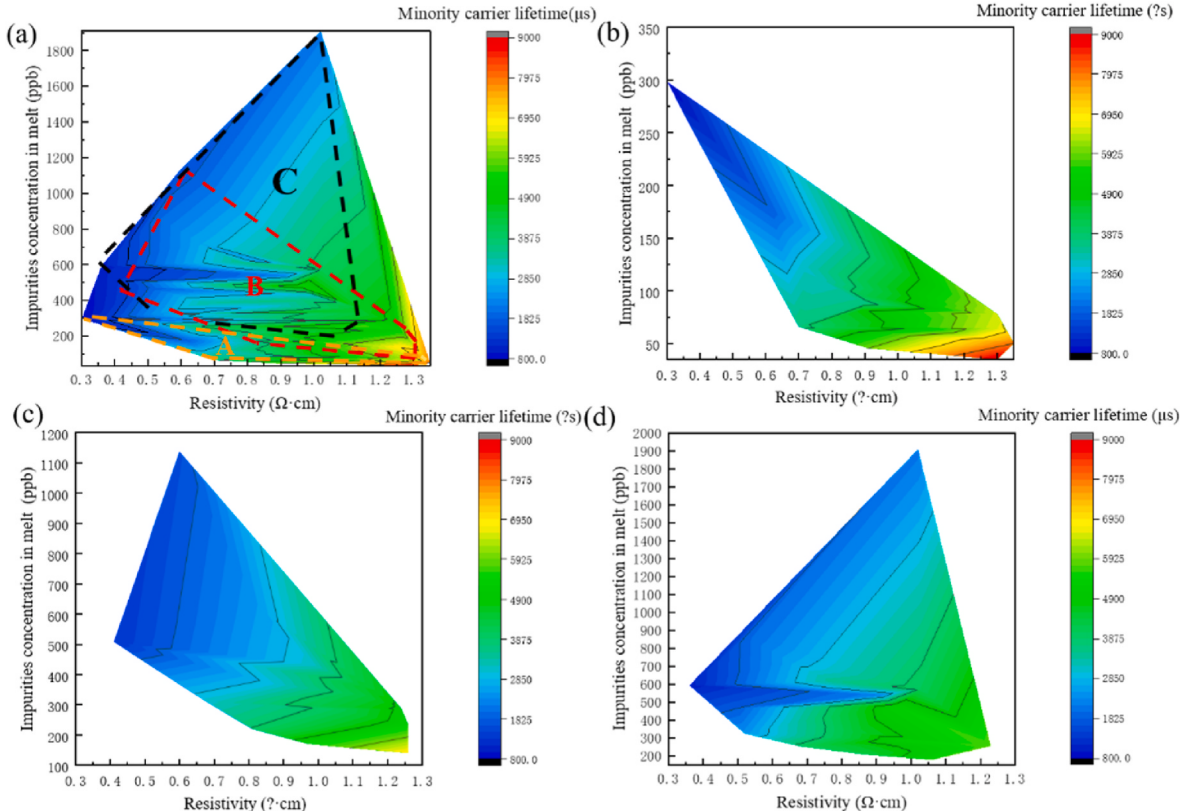


**Fig. 11.** Relationship between impurities concentration in crystal ingot and minority carrier lifetime (a): Comparative analysis chart of minority carrier lifetime; (b): Distribution diagram of minority carrier life of ingots produced from Group A; (c): Distribution diagram of minority carrier life of ingots produced from Group B; (d): Distribution diagram of minority carrier life of ingots produced from Group C.

26–29]. Based on the efficiency verification results, ring defects of varying degrees were observed during the EL test process in groups B and C. Group C experienced a greater decrease in efficiency, with a higher proportion of ring defect sheets. It is possible that these two factors are directly related to each other.

Therefore, the location of ring defects in group C was counted separately and re-compared, and the crystal ingots with high impurities concentration were divided into three groups according to their [O<sub>i</sub>]. Higher than 12.9 ppma was high oxygen group, 9.3–12.9 ppma was medium oxygen group, and less than 9.3 ppma was low oxygen group. The statistical range was all within the same solidification ratio.

As shown in Table 5, there is a significant difference in efficiency and proportion of ring defects among the three groups. Ring defects were exclusively observed in the high oxygen group, accounting for a significant proportion of 13%. However, no ring defects were observed in either the medium oxygen group or the low oxygen group. As for efficiency, the high oxygen group experienced a 0.29% decrease compared to the low oxygen group, whereas the medium oxygen group only experienced a 0.06% decrease. The appearance of ring defects in the high oxygen group had a significant impact on the decline in efficiency. For high-efficiency N-type monocrystalline silicon cells, the difference in electrical performance of the crystal ingots grown by high and low impurities concentration feedstock mainly come from the minority carrier recombination center dominated by ring defects.

For ring defects that have a great influence on the electrical properties, most studies believe that they were only related to the oxygen in Cz monocrystalline silicon. Basnet et al. characterized it by high-resolution Fourier transform infrared spectroscopy and high-resolution PL [17]. It was considered that it was oxygen precipitation with multiple continuous high-density recombination centers, and Nauka et al. proposed that it had a quantitative relationship with [O<sub>i</sub>], and the minority carrier lifetime was lower when the [O<sub>i</sub>] was higher [30].

However, at the same [O<sub>i</sub>], we did not find the same ring defect in group A, so it is speculated that the ring defect is not only determined by the oxygen alone (Please refer to Supplement Material II for detailed testing data). When the impurities concentration was low, oxygen precipitation lacked enough nucleation core. Zhang et al. proposed that for low-carbon Cz silicon crystals, metal impurities such as Fe could promote the formation of oxygen precipitation [31]. Meanwhile, Murphy et al. discovered that the recombination activity of the strained oxide precipitated and surrounding defects is determined by the quantity of segregated iron atoms [32].

During the actual production process, the convex solid-liquid interface during crystal growth, combined with the influence of the solid-liquid interface on impurity segregation distribution in the radial direction, often results in the circular enrichment of metal impurities in the same horizontal region, as shown in Fig. 9 above. The enrichment of metal impurities promotes the nucleation and precipitation of oxygen on them to some degree, forming oxygen precipitation and maintaining the original circular characteristics. Under appropriate heat treatment conditions, these oxygen precipitates grow to form ring defects, leading to a significant decline in electrical properties. Therefore, compared to past experience, it is necessary to focus equally on [O<sub>i</sub>] and metal impurities for the generation of ring defects.

#### 4. Conclusion

In this paper, the electrical properties of N-type RCz silicon prepared from feedstock with different metal impurity concentrations were studied. Through the analysis, the following conclusions are mainly formed.

(1) For an RCz ingot, in the axial direction of the ingot, minority carrier lifetime decreased with the increase of the solidification ratio. There was a big difference in minority carrier lifetime between the head and the tail, mainly due to the influence of the

**Table 5**  
Effect of different [O<sub>i</sub>] on ring defect in group C.

Group	low	Medium	high
[O <sub>i</sub> ] range (ppma)	<9.3	9.3–12.9	>12.9
Eff (%)	24.60	24.54	24.31
Uoc (V)	0.71	0.71	0.71
Isc (A)	11.1	11.0	11.0
FF(%)	83.2	83.2	82.9
Wafer count	17,658	8355	4038
Ring defect Proportion (%)	0	0	13

segregation of metal impurities in silicon. In the radial direction, the distribution of minority carrier lifetime was not much different, and the center was slightly lower than the edge. This is the result of the combination of the convex solid-liquid interface and the segregation of metal impurities.

- (2) In the continuous growth of 4 RCz ingots, the distribution of minority carrier lifetime decreases as the number of ingots increases. According to the content of impurities in the feedstock, the minority carrier lifetime and electrical properties were quite different. Properly broadening the impurity content of feedstock could still maintain the RCz ingots minority carrier lifetime at a relatively high and stable level. In this study, altering the proportion of raw materials and appropriately increasing the metal impurity content did not lead to a significant decrease in electrical performance (Group B). The resulting minority carrier lifetime and battery conversion efficiency reached 6900 μs and 24.57%, respectively.
- (3) In the condition of high oxygen and high impurities, solar cells with ring defects are more likely to be produced. Ring defects had a great influence on the average conversion efficiency of N-type RCz silicon, 13% of solar cells with ring defects in total would lead to the average conversion efficiency lost over 0.29%. Meanwhile, since ring defects are only detected in the high oxygen concentration region of high impurity raw materials, it can be speculated that metal impurities may promote the formation of ring defects by promoting precipitation nucleation. Therefore, the key to suppressing ring defects is to prevent the simultaneous occurrence of high oxygen and high metal impurities.

#### CRediT authorship contribution statement

Zhiqiang Hu: Writing – review & editing, Writing – original draft, Methodology, Investigation, Formal analysis. Mu Cong: Investigation, Formal analysis, Data curation, Conceptualization. Xinyu Zhang: Resources, Project administration, Formal analysis. Jiayan Li: Writing – review & editing. Jiangang Zhang: Investigation, Formal analysis, Conceptualization. Yi Tan: Project administration. Ziyang Ou: Resources, Data curation. Yangjun Chen: Resources, Project administration. Changming Liu: Resources, Formal analysis. Dachuan Jiang: Methodology, Formal analysis. Pengting Li: Project administration, Methodology, Investigation, Funding acquisition, Formal analysis, Data curation, Conceptualization.

#### Declaration of competing interest

The authors declare that they have no known competing financial interests or personal relationships that could have appeared to influence the work reported in this paper.

#### Data availability

Data will be made available on request.

## Acknowledgement

The authors gratefully acknowledge the Project Supported by the National Natural Science Foundation of China (51974057), the Science and Technology Innovation Fund of Dalian (Grant No. 2019RT13).

## Appendix A. Supplementary data

Supplementary data to this article can be found online at <https://doi.org/10.1016/j.solmat.2023.112482>.

## References

- [1] Energy Institute, 72<sup>nd</sup> statistical review of wod energy, See, <https://www.energyinstitute.org/statistical-review/resources-and-data-downloads>, 2022.
- [2] A. Sharif, M.S. Meo, M. Chowdhury, K. Sohag, Role of solar energy in reducing ecological footprints: an empirical analysis, *J. Clean. Prod.* 292 (26) (2021), 126028.
- [3] O. Usman, S.S. Akadiri, I. Adeshola, Role of renewable energy and globalization on ecological footprint in the USA: implications for environmental sustainability, *Environ. Sci. Pollut. Control Ser.* 27 (24) (2020) 30681–30693, <https://doi.org/10.1007/s11356-020-09170-9>.
- [4] C. Ballif, F.-J. Haug, M. Boccard, P.J. Verlinden, G. Hahn, Status and perspectives of crystalline silicon photovoltaics in research and industry, *Nat. Rev. Mater.* 7 (8) (2022) 597–616, <https://doi.org/10.1038/s41578-022-00423-2>.
- [5] G.M. Wilson, M. Al-Jassim, W.K. Metzger, S.W. Glunz, P. Verlinden, G. Xiong, L. M. Mansfield, B.J. Stanberry, K. Zhu, Y. Yan, J.J. Berry, A.J. Ptak, F. Dimroth, B. M. Kayes, A.C. Tamboli, R. Peibst, K. Catchpole, M.O. Reese, C.S. Klinga, P. Denholm, M. Morjaria, M.G. Deceglie, J.M. Freeman, M.A. Mikofski, D. C. Jordan, G. Tamizhmani, D.B. Sulas-Kern, The 2020 photovoltaic technologies roadmap, *J. Phys. Appl. Phys.* 53 (49) (2020), 493001, <https://doi.org/10.1088/1361-6463/ab9c6a>.
- [6] International Energy Agency, Trends in PV applications. [https://iea-pvps.org/trends\\_reports/trends-2022/](https://iea-pvps.org/trends_reports/trends-2022/), 2022.
- [7] B. Singha, C.S. Solanki, N-type solar cells: advantages, issues, and current scenarios, *Mater. Res. Express* 4 (7) (2017), <https://doi.org/10.1088/2053-1591/aa6402>.
- [8] J. Schmidt, B. Lim, D. Walter, K. Bothe, S. Gatz, T. Dullweber, P.P. Altermatt, Impurity-related limitations of next-generation industrial silicon solar cells, *IEEE J. Photovolt.* 3 (1) (2013) 114–118, <https://doi.org/10.1109/jphotovol.2012.2210030>.
- [9] F. Zhu, D. Wang, J. Bian, J. Liu, Z. Liu, Phosphorous diffusion gettering of n-type CZ silicon wafers for improving the performances of silicon heterojunction solar cells, *Sol. Energy Mater. Sol. Cell.* 157 (2016) 74–78, <https://doi.org/10.1016/j.solmat.2016.05.023>.
- [10] A. Liu, S.P. Phang, D. Macdonald, Gettering in silicon photovoltaics: a review, *Sol. Energy Mater. Sol. Cell.* 234 (2022), 111447, <https://doi.org/10.1016/j.solmat.2021.111447>.
- [11] D. Yang, D. Li, L. Wang, X. Ma, D. Que, Oxygen in Czochralski silicon used for solar cells, *Sol. Energy Mater. Sol. Cell.* 72 (1–4) (2002) 133–138.
- [12] S. Singh, O. Prakash, Formation of oxygen related donors during transition from thermal donors to new donors in CZ-silicon, in: 3rd Annual SPIE Conference on Optical Characterization Techniques, Austin, Tx, 1996, pp. 70–78.
- [13] K. Tanahashi, T. Tachibana, K. Sueoka, M. Moriya, Y. Kida, S. Ustunomiya, K. Shirasawa, H. Takato, Effect of oxygen precipitation in silicon wafer on electrical characteristics of fully ion-implanted n-type PERT solar cells, *Ecs J. Solid State Sci. Technol.* 8 (10) (2019) P596–P601, <https://doi.org/10.1149/2.0191910jss>.
- [14] H. Sun, C. Liu, Q. Hao, L. Wang, Effect of oxygen precipitates in solar grade silicon on minority carrier lifetime and efficiency of solar cells, *Rare Met.* 25 (2006) 141–145, [https://doi.org/10.1016/s1001-0521\(07\)60061-8](https://doi.org/10.1016/s1001-0521(07)60061-8).
- [15] Talid Sinno, Point defect dynamics and the oxidation-induced StackingFault ring in czochralski-grown silicon crystals, *J. Electrochem. Soc.* 145 (1) (1998) 302–318.
- [16] J. Haunschild, I.E. Reis, J. Geilker, S. Rein, Detecting efficiency-limiting defects in Czochralski-grown silicon wafers in solar cell production using photoluminescence imaging, *Phys. Status Solidi Rapid. Lett.* 5 (5–6) (2011) 199–201, <https://doi.org/10.1002/pssr.201105183>.
- [17] R. Basnet, C. Sun, H. Wu, H.T. Nguyen, F.E. Rougieux, D. Macdonald, Ring defects in n-type Czochralski-grown silicon: a high spatial resolution study using Fourier-transform infrared spectroscopy, micro-photoluminescence, and micro-Raman, *J. Appl. Phys.* 124 (24) (2018), <https://doi.org/10.1063/1.5057724>.
- [18] A.A. Istratov, T. Buonassisi, R.J. McDonald, A.R. Smith, R. Schindler, J.A. Rand, J. P. Kalejs, E.R. Weber, Metal content of multicrystalline silicon for solar cells and its impact on minority carrier diffusion length, *J. Appl. Phys.* 94 (2003).
- [19] D. Macdonald, A. Cuevas, A. Kinomura, Y. Nakano, Phosphorus gettering in multicrystalline silicon studied by neutron activation analysis, in: Conference Record of the IEEE Photovoltaic Specialists Conference, 2002, pp. 285–288.
- [20] G. Coletti, Sensitivity of state-of-the-art and high efficiency crystalline silicon solar cells to metal impurities, *Prog. Photovoltaics Res. Appl.* 21 (5) (2013) 1163–1170, <https://doi.org/10.1002/pip.2195>.
- [21] G. Coletti, R. Kvande, V.D. Mihailetti, L.J. Geerligs, L. Arnberg, E.J. Øvrelied, Effect of iron in silicon feedstock on p- and n-type multicrystalline silicon solar cells, *J. Appl. Phys.* 104 (10) (2008) 677.
- [22] T. Nishinaga, Handbook of Crystal Growth, Springer Berlin Heidelberg, 2015.
- [23] P. Haesen, J.M. Galligan, *Phys. Metall., Phys. Today* 31 (12) (1978) 51–52.
- [24] R.J. Davis Jr., A. Rohatgi, H.R. Hopkins, D.P. Blais, Rai-Choudhury, Impurities in silicon solar cells, *Electron Devices, IEEE Trans.* 27 (4) (1980) 677–687.
- [25] G.W. Pfann, Zone melting, *Metall. Rev.* 2 (1) (1962) 29–76.
- [26] G. Coletti, P. Manshanden, S. Bernardini, P.C.P. Bronsveld, A. Gutjahr, Z. Hu, G. Li, Removing the effect of striations in n-type silicon solar cells, *Sol. Energy Mater. Sol. Cell.* 130 (2014) 647–651, <https://doi.org/10.1016/j.solmat.2014.06.016>.
- [27] G. Gaspar, G. Coletti, M. Juel, S. Würzner, R. Søndenå, M. Di Sabatino, L. Arnberg, E.J. Øvrelied, Identification of defects causing performance degradation of high temperature n-type Czochralski silicon bifacial solar cells, *Sol. Energy Mater. Sol. Cell.* 153 (2016) 31–43, <https://doi.org/10.1016/j.solmat.2016.04.008>.
- [28] Z. Wang, X. Zhu, S. Yuan, X. Yu, D. Yang, Comprehensive characterization of efficiency limiting defects in the swirl-shaped region of Czochralski silicon, *Sol. Energy Mater. Sol. Cell.* 236 (2022), <https://doi.org/10.1016/j.solmat.2021.111533>.
- [29] K. Marsden, S. Sadamitsu, T. Yamamoto, Tatsuhiko Shigematsu, generation of oxidation-induced stacking faults in czochralski-grown silicon crystals exhibiting a ring-like distributed stacking fault region, *Jpn. J. Appl. Phys.* 34 (Part 1, No. 6A) (1995) 2974–2980.
- [30] Nauka, Oxygen-induced recombination centers in as-grown Czochralski silicon crystals, *Appl. Phys. Lett.* 43 (3) (1983) 241–243.
- [31] Y. Zhang, Effect of Fe on oxygen and carbon precipitations in silicon, *J. Semiconduct.* 8 (3) (1987) 300–304.
- [32] J.D. Murphy, K. Bothe, V.V. Voronkov, R.J. Falster, On the mechanism of recombination at oxide precipitates in silicon, *Appl. Phys. Lett.* 102 (4) (2013) 499.